Acta Crystallographica Section D
Biological Crystallography
ISSN 0907-4449

Structure of a liganded type 2 non-specific lipid-transfer protein from wheat and the molecular basis of lipid binding

François Hoh,[a] Jean-Luc Pons,[a] Marie-Françoise Gautier,[b] Frédéric de Lamotte[b] and Christian Dumas[a]*

[a]Centre de Biochimie Structurale, CNRS UMR5048–INSERM U554, 29 Rue de Navacelles, 34090 Montpellier, France, and [b]Polymorphismes d'Intérêt Agronomique, INRA UMR 1096, 2 Place Viala, 34060 Montpellier CEDEX 01, France

Correspondence e-mail: dumas@cbs.cnrs.fr

Received 14 October 2004
Accepted 5 January 2005

PDB Reference: wheat ns-LTP2, 1tuk, r1tuksf.

In plants, a family of ubiquitous proteins named non-specific lipid-transfer proteins (ns-LTPs) facilitates the transfer of fatty acids, phospholipids and steroids between membranes. Recent data suggest that these secreted proteins play a key role in the formation of cuticular wax layers and in defence mechanisms against pathogens. In this study, X-ray crystallography has been used to examine the structural details of the interaction between a wheat type 2 ns-LTP and a lipid, L-α-palmitoyl-phosphatidyl glycerol. This crystal structure was solved *ab initio* at 1.12 Å resolution by direct methods. The typical α-helical bundle fold of this protein is maintained by four disulfide bridges and delineates two hydrophobic cavities. The inner surface of the main cavity is lined by non-polar residues that provide a hydrophobic environment for the palmitoyl moiety of the lipid. The head-group region of this lipid protrudes from the surface and makes several polar interactions with a conserved patch of basic residues at the entrance of the pocket. The alkyl chain of a second lipid is bound within an adjacent smaller cavity. The structure shows that binding of the lipid tails to the protein involves extensive hydrophobic interactions.

1. Introduction

Plant non-specific lipid-transfer proteins (ns-LTPs) are small soluble proteins that have the ability to enhance *in vitro* the inter-membrane exchange and transfer of various amphiphilic molecules including phospholipids, glycolipids, steroids, acylCoA and fatty acids. They have been isolated from a number of plant species and form a multigene family (Kader, 1996). Within this large family of proteins, two classes of ns-LTPs have been described. Both are secreted proteins with a hydrophobic N-terminal signal sequence. They exhibit a basic isoelectric pH and a homologous all-helical fold stabilized by four disulfide bridges. Type 1 proteins are distinct from type 2 proteins in terms of protein sequence (less than 30% similarity), molecular weight (7 kDa, ~60 amino acids for type 2 and 9 kDa, ~90 amino acids for type 1) and biological properties (Kader, 1996; Douliez *et al.*, 2000). They play several *in vivo* roles, including the transport and assembly of cutin and suberin components (Hollenbach *et al.*, 1997) and the defence of plants against pathogens (Molina *et al.*, 1993; Garcia-Olmedo *et al.*, 1995). It has been shown that the differential expression of these *ltp* genes in various tissues is also regulated by several environmental factors such as osmotic stress (Kader, 1996) and cold (Molina *et al.*, 1996).

The antifungal and antibacterial functions of ns-LTPs are now well established for several species both *in vitro* and *in vivo* (Garcia-Olmedo *et al.*, 1995; Maldonado *et al.*, 2002).

Table 1
Statistics of data collection and refinement.

Values in parentheses refer to the last resolution shell (1.16–1.12 Å).

Data collection	
Space group	*C*2
Unit-cell parameters	
a (Å)	61.46
b (Å)	29.23
c (Å)	41.55
β (°)	127.65
Wavelength (Å)	0.8000
Resolution (Å)	32.9–1.12
Measured reflections	166777
Unique reflections	22535 (1389)
$R_{\rm fac}$ (%)	9.4 (28.0)
Redundancy	6.8 (4.6)
Completeness (%)	94.8 (84.7)
$\langle I/\sigma(I)\rangle$	18.9 (3.8)
Refinement	
Resolution range (Å)	32.9–1.12
Reflections (total/free)	22496/1097
$R_{\rm fac}$ (including test reflections)	13.8 (24.4)
$R_{\rm work}$ (excluding test reflections)	13.7 (24.4)
$R_{\rm free}$ (test reflections)	16.2 (24.8)
No. of atoms	
Total non-H	621
Protein/water	498/79
Ions/lipid ligands	2/42
B factors (Å^2)	
Overall	12.0
Main-chain atoms	10.1
Side-chain atoms	13.8
Lipids/water ions	25.0/25.0
R.m.s. deviations from ideal values	
Bonds distances (Å)	0.021
Bond angles (°)	1.93
Chiral volumes (Å^3)	0.13
Ramachandran plot: most favoured/allowed (%)	100.0
Overall coordinate errors (Å)	0.016

However, the underlying molecular mechanisms are not clearly understood (Blein *et al.*, 2002). These proteins are up-regulated upon response to infection by phytopathogens. Overexpression of a barley ns-LTP1 in *Arabidopsis* and tobacco transgenic plants enhances tolerance to fungal pathogens (Molina & Garcia-Olmedo, 1997). Ns-LTPs could be involved in disease-resistance signalling transduction as specific lipid sensors (Maldonado *et al.*, 2002) and as competitors with elicitins for plasma-membrane receptors (Buhot *et al.*, 2001; Blein *et al.*, 2002). Ns-LTPs have numerous potent applications either in pharmacology (Pato *et al.*, 2001) or agro-industries (Douliez *et al.*, 2000) and have also been frequently identified as plant pan-allergens present in foods and pollens (Marion *et al.*, 2003).

Three-dimensional structures have been determined for ns-LTP1 from wheat, rice, maize and barley seeds in both unliganded and complexed forms with lipids (Gincel *et al.*, 1994; Shin *et al.*, 1995; Gomar *et al.*, 1996; Heinemann *et al.*, 1996; Lerche *et al.*, 1997, 1998; Lee *et al.*, 1998; Charvolin *et al.*, 1999; Han *et al.*, 2001). They are characterized by a central hydrophobic tunnel into which the alkyl moiety of lipids is inserted. In type 1 ns-LTPs, this large tunnel can accommodate up to two monoacylated lipids in a head-to-tail orientation (Charvolin *et al.*, 1999). Although NMR structures of unliganded (Samuel *et al.*, 2002) and liganded (Pons *et al.*, 2003) forms of ns-LTP2 have been reported, significant differences in their tertiary fold and a lack of details of the lipid–protein interactions justify further structure–function studies. We have now utilized a different technique, X-ray crystallography, to assess the three-dimensional structure of a liganded wheat ns-LTP2 in order to gain a deeper understanding of its lipid-transfer function. Unexpectedly, the structure revealed two independent lipid-binding sites and a dimeric arrangement. The details of the interactions between the molecules of the L-α-palmitoyl-phosphatidyl glycerol and the protein are described at atomic resolution and provide further insight into the lipid-binding mechanisms.

2. Materials and methods

2.1. Protein expression and purification

Recombinant wheat (*Triticum aestivum*) ns-LTP2 was produced with the *Pichia pastoris* transformant GS115-Tdltp18-tr5.2 (De Lamotte *et al.*, 2001) and purified as previously described (Pons *et al.*, 2003). The lyophilized protein was dissolved in 20 m*M* MES buffer pH 6.0 containing 1 m*M* NaN_3. The ns-LTP2 and L-α-palmitoyl-phosphatidyl glycerol (LPG) stock solutions were mixed to give a lipid: protein molar ratio of 3:2. The resulting complex was then concentrated to 35 mg ml^{-1} using a 3 kDa molecular-weight cutoff ultrafiltration device. The high level of purity and homogeneity of the sample were verified by mass-spectrometry analysis.

2.2. Analytical size-exclusion chromatography

The recombinant wheat ns-LTP2 was characterized by analytical size-exclusion chromatography on a Superdex 75 HR 10/30 column (Amersham Biosciences). 100 µl aliquots at 2 mg ml^{-1} in 50 m*M* MES buffer pH 6 were loaded at a 0.5 ml min^{-1} flow rate. The column was calibrated using an Amersham Biosciences LMW calibration kit and corn kernel trypsin inhibitor (MW 13 500 Da).

2.3. Crystallization and data collection

Crystals of the liganded wheat ns-LTP2 were obtained by the vapour-diffusion method using sitting drops. The optimal reservoir solution contains 100 m*M* sodium citrate buffer pH 6.0–6.5, 30%(*w*/*v*) PEG 6000 and 1.0 *M* LiCl. Microcrystals were observed at 291 K after two weeks and high-quality crystals grow in approximately three to five months to average dimensions of 0.15 × 0.15 × 0.07 mm. After a short soak in cryoprotective solution containing 0.25 *M* KI (Dauter *et al.*, 2000), high-resolution diffraction data were collected from a single cryocooled crystal (100 K) using the BM14 beamline (ESRF, Grenoble) and a MAR Research CCD detector. The wavelength was tuned to 0.8 Å and the crystal-to-detector distance set as short as possible (100 mm) to achieve atomic resolution. Data to a maximum resolution of 1.12 Å were autoindexed and processed with *MOSFLM* (Leslie, 1999). Scaling and merging were performed with *SCALA* from the

*CCP*4 suite (Collaborative Computational Project, Number 4, 1994). The crystal belongs to the monoclinic *C*2 space group and the unit-cell volume suggests the presence of one protein molecule in the asymmetric unit with 29% solvent content. Data-collection statistics are summarized in Table 1.

2.4. Structure solution

All attempts to solve the structure by molecular replacement with *AMoRe* (Navaza, 1994), *MOLREP* (Vaguine & Teplyakov, 1997) and *EPMR* (Kissinger *et al.*, 1999) using as a probe either the ns-LTP2 NMR models (PDB codes 1n89 and 1l6h) or X-ray models of ns-LTP1s (PDB codes 1rzl and 1fk5) were unsuccessful. Instead of using the weak anomalous signal from iodide at 15.5 keV (Dauter *et al.*, 2002), the structure was ultimately solved by direct methods using the *ab initio* dual-space recycling procedure called the *Shake and Bake* method (Weeks & Miller, 1999*a*) and implemented in the *SnB* program (Weeks & Miller, 1999*b*). Normalized structure-factor magnitudes ($|E|$ values) were computed using the program *DREAR* (Blessing & Smith, 1999). The 5190 reflections with the highest $|E|$ values were used to generate 110 000 triplet structure invariants. Working with default parameters, *SnB* generated 1000 trial structures that were subjected to 520 cycles of phase refinement. A total of about 620 peaks were selected from the *E* maps for real-space recycling. Of the 1000 random initial sets of trial phases processed, 40–50 yielded possible solutions. One of the most successful trials with an $R_{\rm min}$ of 0.438 was examined in detail. The corresponding electron-density map generated with this procedure was of high quality and included peaks corresponding to nearly all of the non-H atoms of the wheat ns-LTP2.

2.5. Model building and refinement

The complete atomic model was built using the automatic *ARP*/*wARP* procedure (Perrakis *et al.*, 1997) starting from the atom sites generated from *SnB*. The protein structure refinement was performed with the program *REFMAC*5 (Murshudov *et al.*, 1997). Model adjustments performed in *O* (Jones *et al.*, 1991) were based on $2F_{\rm o} - F_{\rm c}$ and $F_{\rm o} - F_{\rm c}$ σ_A-weighted electron-density maps (Read, 1986). Restrained maximum-likelihood refinement in *REFMAC*5 started with 2.0 Å data and the resolution was quickly extended in a stepwise procedure to include all reflections in the 32.9–1.12 Å range without any σ-cutoff. The weighting parameter between the X-ray and geometric terms of the refinement residual was gradually increased from 0.5 to 5 to loosen the stereochemical constraints. Additional peaks with excellent density and clear interpretation were included as water molecules, iodide ions or modelled as alternate conformations for side chains. Two typical features in the electron-density map that could not be attributed to the protein were unambiguously modelled in one case as a complete molecule of LPG and in the other case as a portion of the acyl tail of a second lipid. Several rounds of refinement were performed to introduce restrained anisotropic displacement parameters (ADPs) for the protein atoms, reducing the $R_{\rm work}$ and $R_{\rm free}$ factors by 2.0 and 1.8%, respectively. The final refinement steps, in which the test reflections were included, converged at an *R*-factor value of 13.8%. The refinement statistics are summarized in Table 1.

2.6. The final model

The stereochemistry, geometry and quality of the structure were assessed using *PROCHECK* (Laskowski *et al.*, 1993) and

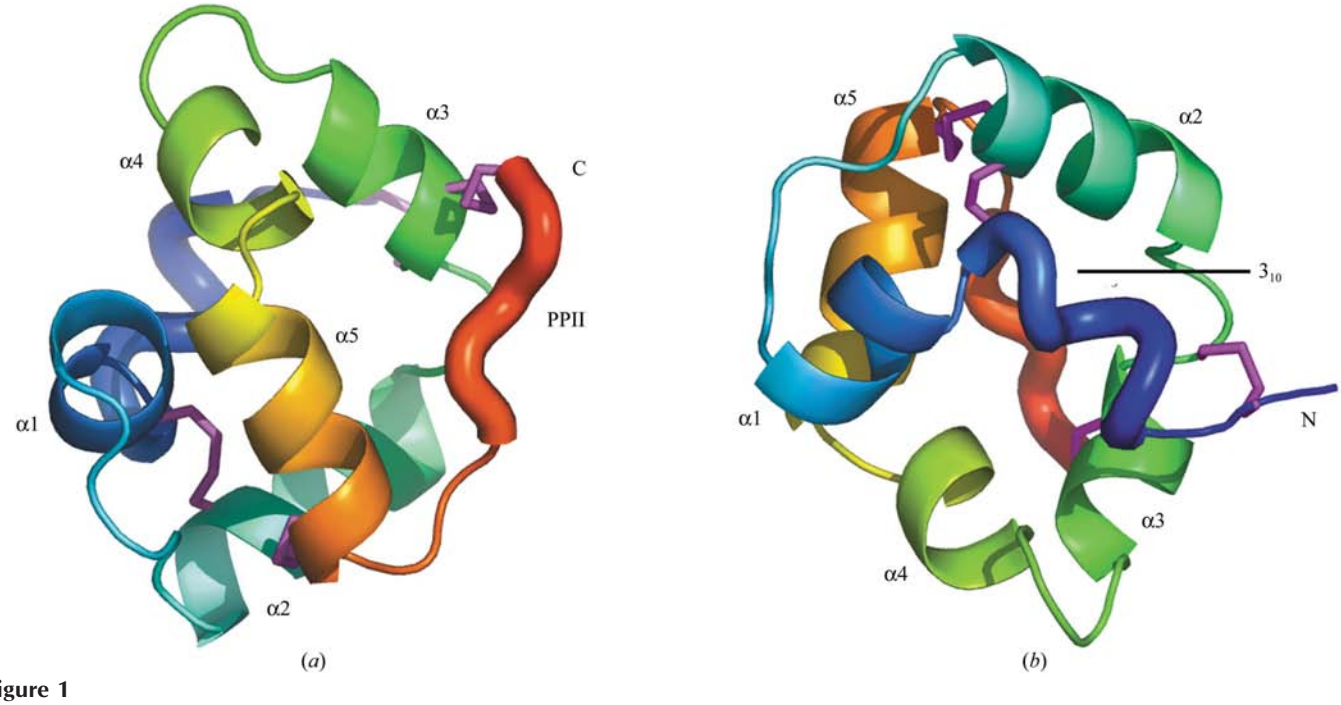

Figure 1
Overall structure of the wheat ns-LTP2. The α-helices are labelled α1–α5. The N-terminal 3_{10}-helix is coloured dark blue and the C-terminal polyproline type II helix orange. The cysteine side chains forming the four disulfide bridges are coloured magenta and represented as stick models. The two orthogonal views (*a*) and (*b*) were drawn with *PyMOL* (DeLano, 2002).

SFCHECK (Vaguine *et al.*, 1999). The Ramachandran plot shows 100% of residues to be in the core region. The anisotropic displacement parameters were analyzed using the program *PARVATI* (Merritt, 1999). Solvent-accessible areas were calculated with *AREAIMOL* (Collaborative Computational Project, Number 4, 1994) with a probe radius of 1.4 Å.

3. Results

3.1. Structure determination

We were able to grow diffracting crystals of recombinant wheat ns-LTP2 liganded to the LPG lipid in space group *C*2. The crystal structure was solved by *ab initio* direct methods, *i.e.* from the single-wavelength data without the use of known fragments or the weak anomalous signal of bound iodide ions, and refined at 1.12 Å resolution (Table 1). The efficient combination of the *SnB* (Weeks & Miller, 1999*b*), *ARP*/*wARP* (Perrakis *et al.*, 1997) and *REFMAC*5 (Murshudov *et al.*, 1997) programs allowed the easy solution of the very accurate model of this liganded protein. The final ns-LTP2 structure refined at cryogenic temperature contains 498 non-H protein atoms, two lipid ligands, two iodide anions and 79 water molecules. The density maps for Gln31, Asp41, Ile48, Arg54 and Ser59 clearly showed the presence of alternate conformations. The presence of a fully occupied I atom site and eight S atoms with low *B* factors certainly helped in the seeding procedure and thus reinforced the phasing power of direct methods.

3.2. Overall protein structure

Wheat ns-LTP2 adopts a globular structure with overall dimensions of about 28 × 22 × 20 Å consisting of one N-terminal 3_{10}-helix, five α-helices designated α1–α5 and a short polyproline type II C-terminal helical segment. As shown in Fig. 1, the core of the structure is organized as a helical bundle stabilized by four disulfide bridges. The N-terminal segment containing the 3_{10}-helix (Ala4–Cys10) is anchored to this bundle by two disulfide bridges, Cys2–Cys34 and Cys10–Cys24. The successive helices 3_{10}, α1 (Ala11–Ser16), α2 (Gly22–Gln31), α3 (Phe35–Tyr38), α4 (Gly45–Ile48) and α5 (Pro51–Ser59) pack into a globular structure and delineate a deep hydrophobic cavity. A type-I β-turn is observed between helices α2 and α3. Helices α3 and α4 are connected by an α-turn that is stabilized by hydrogen bonds between the two alternate conformations of the Asp41 side chain and the main-chain NH groups of Thr43 and Tyr44. This canonical hydrogen-bonded α-turn has favoured residues Asp and Pro occurring at positions *i* and *i* + 1, respectively (Dasgupta *et al.*, 2004). The C-terminal region (Leu62–His66) containing the conserved Pro65 residue adopts a polyproline type 2 (PPII) helical conformation, a left-handed helix with three residues per turn (Stapley & Creamer, 1999). This segment is anchored to the helical bundle by the Cys36–Cys67 and Cys25–Cys60 disulfide bridges and by a hydrogen bond between the main-chain NH group of Leu62 and the carbonyl of Leu57.

This highly stable protein fold is maintained by an extensive hydrogen-bonding network and four strictly conserved disulfide bridges. Their C—S—S′—C torsion angles show a classical left-handed conformation (−78, −75 and −81° for Cys2–Cys34, Cys25–Cys60 and Cys36–Cys67, respectively), except for one (Cys10–Cys24) which has the less favoured right-handed configuration (111°). The inter- and intra-helical hydrogen-bond network, involving capped helices, stable turns and numerous water-mediated hydrogen bonds, also contributes to the high stability of this compact fold as demonstrated by thermal (T_m > 368 K) and guanidine-induced unfolding experiments on rice ns-LTP2 (Samuel *et al.*, 2002).

Searches in non-redundant protein sequence databases using the wheat ns-LTP2 sequence identified about 40 proteins with significant homology scores, from 60 to 98% sequence identity. As illustrated in Fig. 2, a representative subset of these aligned sequences contains a number of invariant and highly conserved amino acids consistent with a common fold.

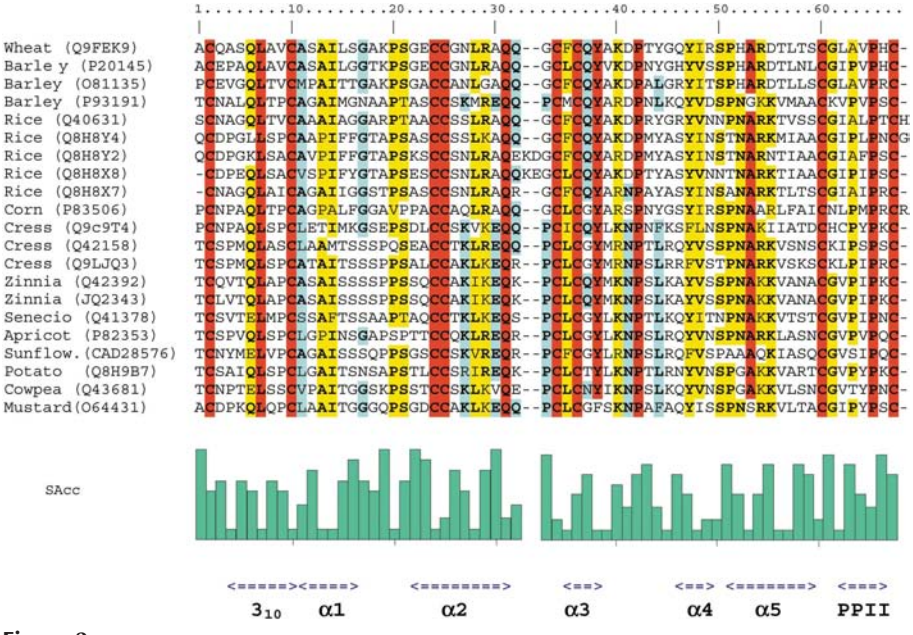

Figure 2
Sequence alignments, secondary-structure elements and surface exposure of ns-LTP2s. Gaps are denoted by dashes. Strictly conserved residues are shown in red boxes and strongly and weakly conserved residues in yellow and blue boxes, respectively. For each residue, the green bar is proportional to its solvent-accessibility surface area (SAcc). The secondary-structure assignments deduced from wheat ns-LTP2 crystal structure are displayed below the sequence alignments.

3.3. The hydrophobic cavities

As noted above, the spacial arrangement of the helical bundle and the C-terminal PPII segment creates a large and long cavity that serves as the major

lipid-binding site. This cavity has the shape of an elongated and curved channel of about 17 Å in length and 5 Å in diameter (Fig. 3*a*), as defined by the van der Waals surface of the bordering atoms. The small cavity entrance is surrounded by residues Cys36, Lys40, Arg49, Arg54, His66 and Cys67. Helices α3 (Phe35, Cys36, Tyr38), α4 (Ile48), α5 (Ala53, Arg54, Leu57), the loop α3/α4 (Ala39, Lys40, Pro42) and the C-terminal PPII segment (Val64, Pro65) delineate the walls of the cavity. Finally, the bottom of the cavity is also formed by hydrophobic residues, Leu7 from helix 3_{10}, Ile14 (helix α1) and Leu28 (helix α2). These three residues constitute a dividing wall with a secondary shortened cavity (Fig. 3*a*) covered by hydrophobic residues Ala4, Ala8, Ala11, Leu15, Tyr44, Tyr47 and Ile48. The volumes of the wheat ns-LTP2 main and secondary cavities were estimated using *VOIDOO* (Kleywegt & Jones, 1994) as 300 and 130 Å^3, respectively, when the lipid ligand is removed.

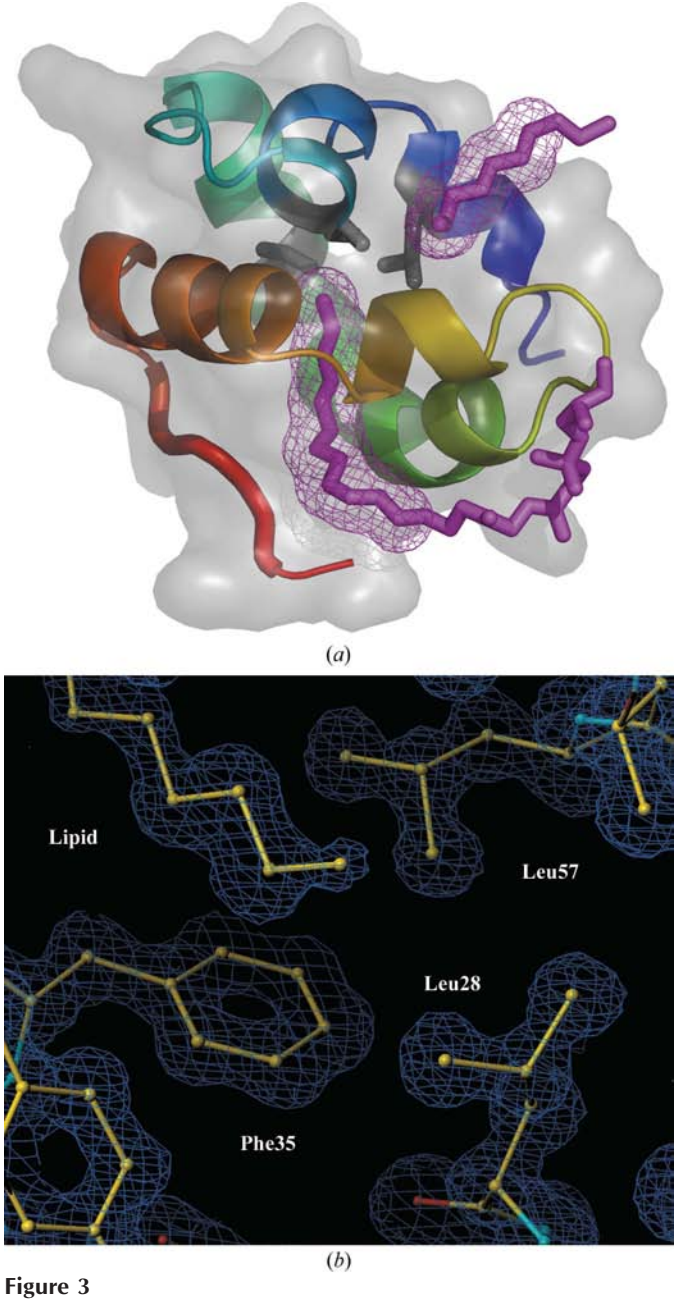

Figure 3
Model of LPG molecules bound to the two hydrophobic cavities of the wheat ns-LTP2 protein. (*a*) Overall structure of the protein displayed as a ribbon model and a molecular surface. The two lipid ligands are displayed as magenta sticks. The van der Waals envelopes of buried acyl chains are represented as a magenta mesh. The residues Leu7, Ile14 and Leu28 forming the septum between the two hydrophobic cavities are shown as grey stick models. (*b*) A view of the electron-density map in the binding pocket is shown superposed with the LPG ligand and the protein model. The final σ_A-weighted map is contoured at 1.1σ (blue).

3.4. Lipid–protein interactions

The electron-density map (Fig. 3*b*) revealed clear densities for two LPG molecules, one buried in the main hydrophobic cavity and the other partially buried at a secondary hydrophobic site. The maximum chain length that could be supported by the electron density in the secondary lipid-binding site is eight C atoms and only these were included in the acyl chain model. The lipid-tail region interacts over a

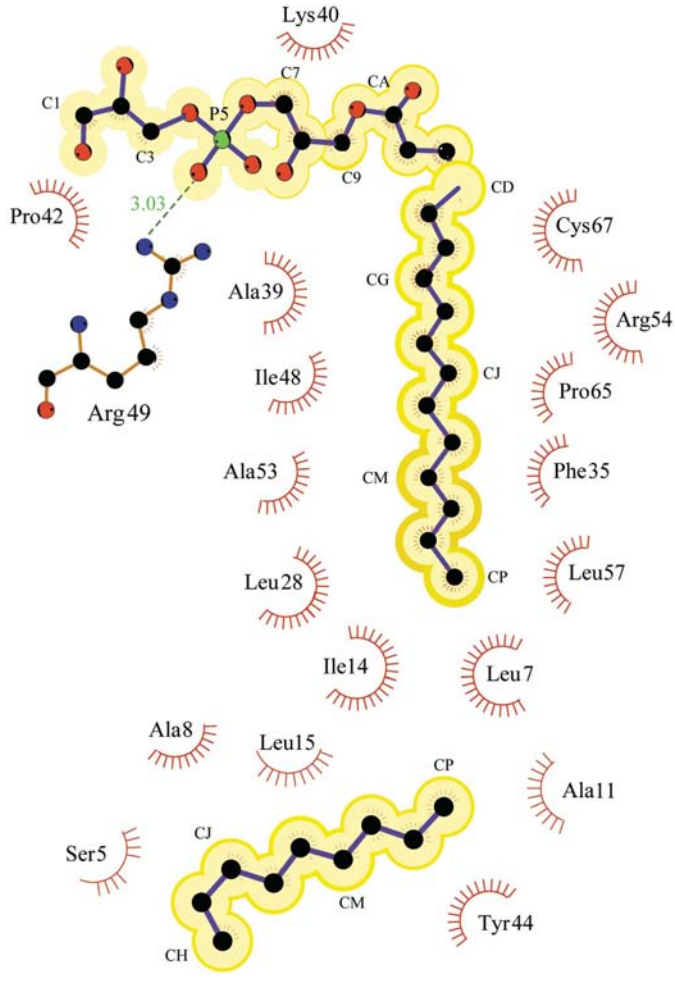

Figure 4
Schematic representation of the binding of the two L-α-palmitoyl-phosphatidyl glycerol lipid ligands to wheat ns-LTP2 protein. Red shading around atoms or residues indicates involvement in hydrophobic contacts. A hydrogen bond is indicated as a green broken line. Ligand bonds are shown in blue. Atoms are colour coded as follows: black, carbon; blue, nitrogen; red, oxygen; green, phosphate. This figure was created with *LIGPLOT* (Wallace *et al.*, 1995).

large surface area within the cavity of the protein, with the closest contacts occurring at the end and the middle of the acyl chain. The hydrophobic contacts between side chains of the ns-LTP2 amino acids lining the cavity and the two lipid molecules are illustrated in Fig. 4. The binding interactions involve atoms from residues Leu7, Ile14, Leu28, Phe35, Ala39, Ile48, Arg49, Ala53, Leu57, Pro65 and Cys67 in the main cavity and Ala4, Ser5, Leu7, Ala8, Ala11, Ile14, Leu15, Tyr44, Tyr47 and Ile48 in the secondary cavity.

The head group of the LPG molecule was located on the surface of the ns-LTP2 molecule (Figs. 3 and 5). It came into close contact with residues from two neighbouring protein molecules in the crystal. Several interactions were observed between the lipid head group and the surrounding protein, in particular between a phosphoryl O atom and the guanidinium group of Arg49. In addition, the LPG makes polar contacts with the Lys40, Pro42 and Arg54 residues and with four water molecules. Total solvent-exposed surface areas of 1000 and 400 Å^2 are buried upon binding of LPG lipids to the main and secondary ns-LTP2 cavities, respectively. The temperature factors of LPG atoms were lowered for the buried acyl tail (13–25 Å^2) and increased progressively (30–45 Å^2) up to the head group.

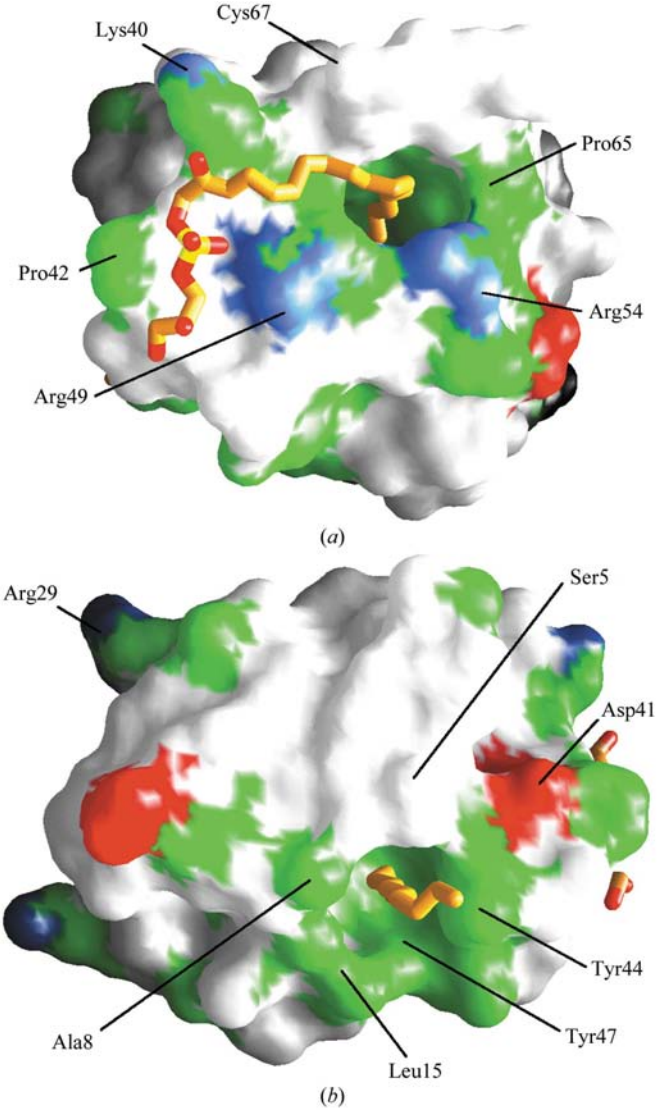

Figure 5
Molecular-surface properties of the wheat ns-LTP2. Hydrophobic areas are shown in green, positively charged residues are coloured blue and negatively charged residues red. The two prominent hydrophobic patches at the entrance and inside the main (*a*) and secondary (*b*) cavities are implicated in lipid-binding sites. The palmitoyl moieties of the lipids are shown as yellow sticks. The surface representations were generated with *GRASP* (Nicholls *et al.*, 1993).

3.5. Protein-surface properties and sequence variability

Fig. 5 shows different views of the molecular surface of the wheat ns-LTP2 coloured according to surface potential (blue, positive; red, negative; green, hydrophobic) with the program *GRASP* (Nicholls *et al.*, 1993). A small cluster of basic residues, Arg49 and the highly conserved residues Lys/Arg40 and Arg/Lys54, located in a groove near the entrance of the main cavity interact with the polar head of the bound LPG. This conserved basic patch anchors the polar head of phospholipids and fatty acids. Two separate regions of highly hydrophobic clusters are seen in Fig. 5. These regions include the wall and the entrance of the primary and secondary lipid-binding cavities. In this ns-LTP2 family, the binding pockets for the lipid are lined by highly conserved residues (Tyr47, Ala53, Pro65 and Cys67), including those forming the septum between the cavities (Leu7, Ile14 and Leu28), and less conserved but hydrophobic residues (Phe35, Ala39, Ile48 and Leu57).

3.6. Packing analysis

The analysis of the crystallographic packing interactions between the adjacent ns-LTP2 molecules reveals a dimeric arrangement involving a crystallographic dyad axis. The most extensive contact between the two molecules involves the

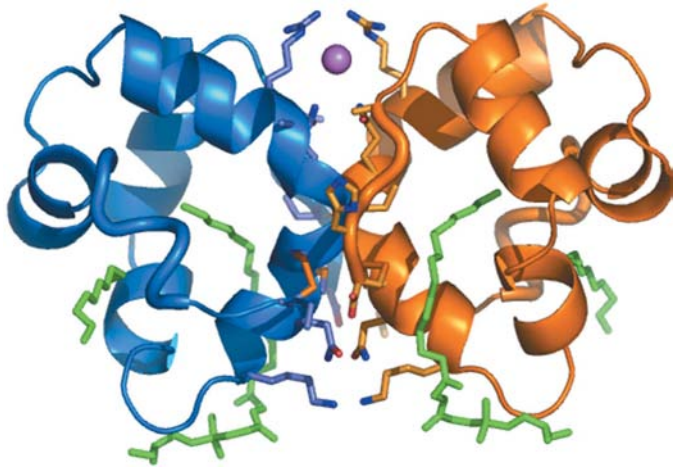

Figure 6
Ribbon diagram of the wheat ns-LTP2 dimer highlighting the key residues involved in the intermolecular interface. The two molecules shown as ribbon models are related by a twofold axis (vertical). The side chains involved at the protein–protein interface are represented as sticks and the iodide ion as a magenta sphere. The lipid ligands are coloured green.

burial of ~600 Å^2 of the surface area per monomer excluding water molecules, which means that approximately 15% of the total solvent-accessible area of each monomer is buried. The total area of the buried surface in the interface represents ~1200 Å^2, a value within the usual range for protein dimers (Bahadur *et al.*, 2004). In this dimeric model illustrated in Fig. 6, the polyproline type II segment of one protomer is juxtaposed with the α2 and α3 helices and the two N-terminal residues of the other protomer. The dimer interface consists of the conserved residues Cys2, Arg/Lys29, Gln31, Cys34, Cys36, Arg/Lys40, Pro65 and Cys67. Our gel-filtration experiments also revealed the presence of two protein species (Fig. 7). These data are consistent with a mixture of dimeric and monomeric forms of ns-LTP2. Therefore, we can reasonably argue that the dimeric pattern of wheat ns-LTP2 in the crystal lattice did not merely arise from packing artifacts and may also exist in solution. It could represent a specific protein–protein interaction that is most likely to be present in concentrated solutions in equilibrium with the monomeric form.

3.7. Water molecules and ions

Besides the polypeptide chain, our refined model includes 79 water molecules and two iodide ions. Of the water molecules, three are in close proximity of the lipid acyl chain near the cavity entry. The first ordered water molecule is buried in the cavity and stacked between the C$^{\gamma}$ atom of Arg54 (2.5 Å) and the C$_L$ atom of LPG (4 Å). This typical buried water located just next the aliphatic hydrocarbon chain in a hydrophobic cavity is frequently observed in the crystal structures of lipid-binding proteins (Lucke *et al.*, 2002) and could represent a residual hydration of the LPG ligand. The second water molecule is located at the entrance of the hydrophobic cavity, in close proximity to the C$_H$ atom of LPG (2.8 Å), and is bound by a hydrogen bond to the Cys67 N atom. The third one is in close proximity of the C$_D$ atom of LPG (2.8 Å) and the main-chain carbonyl of Cys36. These water molecules shield the side chains of the hydrophobic cluster at the top of the cavity from the solvent and presumably affect ligand affinity.

The highest peak (5σ) in the anomalous difference Fourier map corresponds to an I atom and its environment is constituted of residues Ala13 (N atom, 3.9 Å), Ser12 (O$^{\gamma}$ atom, 2.5 Å), Val9 (O atom, 3.8 Å), Ser21 (N atom, 3.75 Å) and two water molecules (3.6 Å). A second partially occupied iodide site localized on a crystallographic twofold axis makes ionic interactions with the guanidinium group of Arg29 and is associated with Gln32 and solvent molecules.

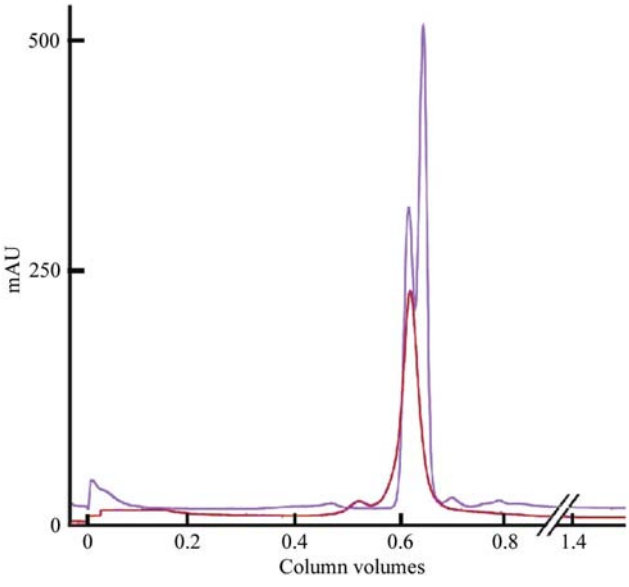

Figure 7
Representative size-exclusion chromatography of wheat ns-LTP2. The elution volumes of the two peaks correspond to a monomer and a dimer of the protein (in magenta). The molecular weight of wheat ns-LTP2 is 6980 Da. The elution volume of corn kernel trypsin inhibitor (PM 13 500 Da) is shown in red.

3.8. Analysis of temperature factors and discrete disorder

The high rigidity of this protein fold is confirmed by almost constant low *B*-factor values for all main-chain atoms of about 10 Å^2, except for the three N-terminal residues (about 20–25 Å^2). The anisotropic displacement parameters show a Gaussian distribution with mean and σ values of 0.56 and 0.14, respectively, for protein atoms. They do not highlight any significant concerted or correlated atomic motions of non-bonded groups. A second conformer was identified for five side chains: Gln31, Asp41, Ile48, Arg54 and Ser59. Except for the case of Ile48, whose rotamer mobility inside the hydrophobic binding cavity could have a functional relevance, these residues are distributed on the surface of the protein and protrude into the solvent channels of the crystal.

3.9. Comparisons with other plant ns-LTP2 and ns-LTP1 structures

Ns-LTP2s constitute a conserved family of proteins (Fig. 2) with a common fold and wide variety of lipid-binding properties. The NMR structures of an unliganded rice ns-LTP2 (Samuel *et al.*, 2002) and a liganded wheat ns-LTP2 (Pons *et al.*, 2003) have been determined recently. Structural alignments of C$^{\alpha}$ atoms for our crystal structure yield r.m.s. deviations of 2.4 Å for 45 C$^{\alpha}$ atoms when compared with the solution structure of the unliganded rice ns-LTP2 (PDB code 1l6h) and an r.m.s. deviation of 2.2 Å for 57 C$^{\alpha}$ atoms when compared with the NMR structure of the same wheat ns-LTP2 (PDB code 1n89). In these NMR models, the cystine C—S—S′—C′ torsional angles are far from the preferred values (Petersen *et al.*, 1999) and have chiralities that are opposite to those of our X-ray model.

The shape of the ligand-binding cavity and the relative orientation of the lipid head group in the crystal and NMR structures of wheat ns-LTP2 are different (Fig. 8*a*). The tunnel-like cavity observed in the NMR structure superimposes well with the two adjacent cavities of the X-ray structure but a single alkyl chain threads through the hydrophobic channel. The proximal and distal entrances of this tunnel correspond to the opening of the main and secondary cavities of the crystal structure, respectively. Moreover, we observed a significant discrepancy in the packing and the

orientation of a number of side-chain residues (Leu7, Leu28, Tyr38, Tyr47 and Ile48) lining the hydrophobic cavity filled with the same LPG lipid. The three neighbouring residues Leu7, Ile14 and Leu28 composing the dividing wall between the cavities of the crystal structure have a different orientation in the NMR structure, allowing the formation of a continuous tunnel rather than spatially separated cavities. The lipid signal could not be unambiguously assigned and the limited number of NOEs observed did not allow a reliable positioning of the acyl chain in the cavity. This may explain the discrepancies in the localization of the LPG lipid. It is interesting to note that unambiguous NOE contacts connect the terminal acyl-chain C_P methyl groups with Tyr44 and Tyr47 and a methylene to Hβ of Phe35 (Pons *et al.*, 2003). These NMR constraints were compatible with the crystal structure, but were not hypothesized as arising from two different lipid molecules. It is noteworthy that the wheat ns-LTP2 sample used for crystallization was obtained following identical expression system and purification procedures as those used for the NMR experiments (Pons *et al.*, 2003). However, the experimental conditions used for crystallization (pH 6.0–6.5, high salt concentration) are different from those used for NMR (pH 3.5, low ionic strength). Thus, these structural differences could be explained both by the limited accuracy of the NMR structure and by distinct conformations of the protein under the two experimental conditions.

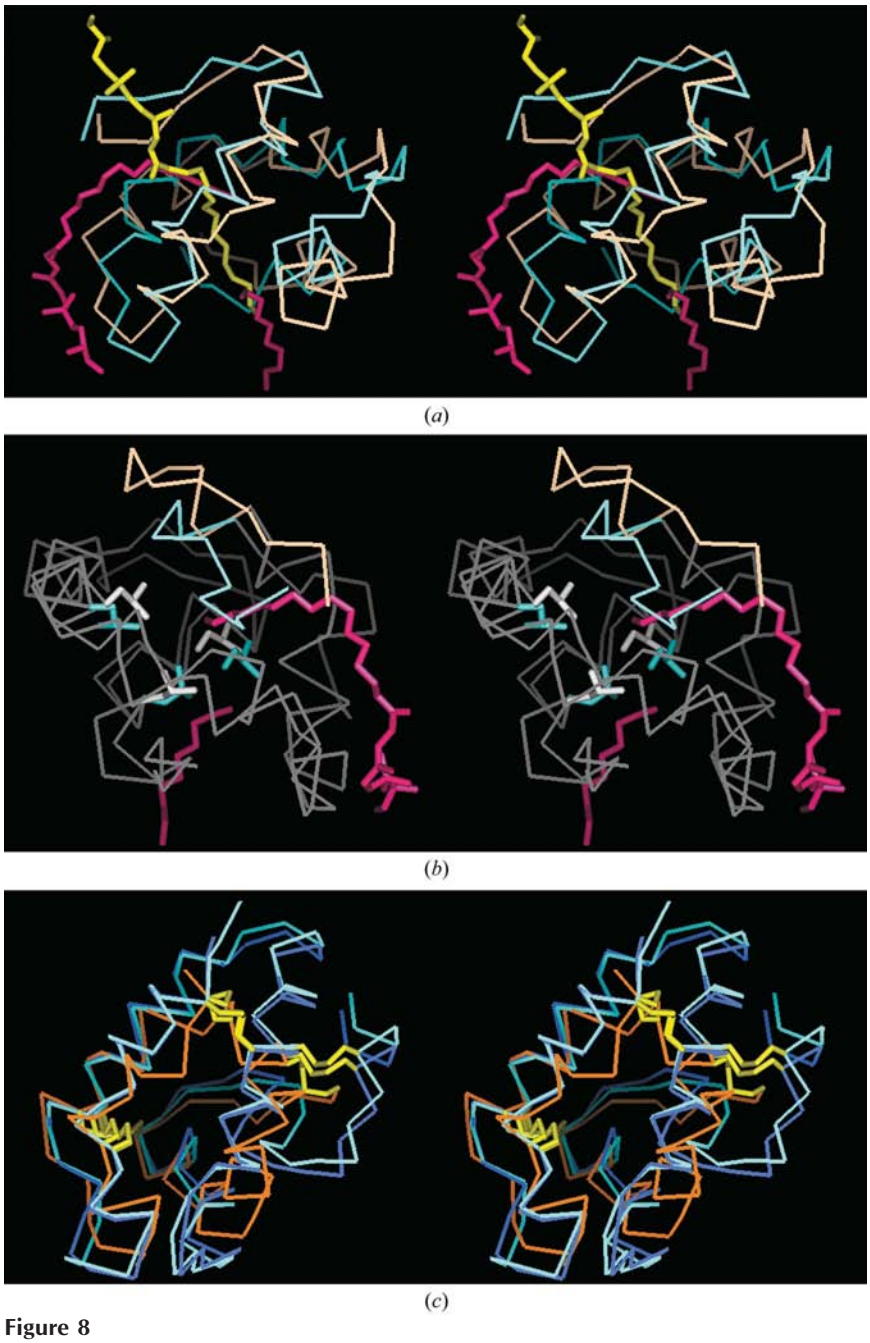

Figure 8
Structural comparisons between ns-LTP1 and ns-LTP2. (*a*) Stereoview of crystal and solution (PDB code 1n89) structures of the liganded wheat ns-LTP2, coloured blue and pink, respectively. The LPG lipid is represented as blue and yellow stick models for the crystal and NMR structures, respectively. (*b*) Superimposition of the crystal structure of liganded wheat ns-LTP2 and the apo form of rice ns-LTP2 (PDB code 1l6h). The C-terminal C^{α} backbone (residues 56–67) and septum residues (Leu7, Ile14 and Leu28) are coloured in beige and blue for apo and liganded ns-LTP2, respectively. (*c*) Superimposition of the crystal structures of wheat ns-LTP2 (orange), ns-LTP1 (PDB code 1bw0, light blue) and maize ns-LTP1 (PDB code 1fk3, dark blue). The cysteine residues are represented as yellow ball-and-stick models.

Comparison of the structures of rice and wheat ns-LTP2 in the free and bound forms shows a major conformational change in the C-terminal region (residues 56–67). As illustrated in Fig. 8(*b*), this C-terminal segment and, to a lesser extent, the last α-helix are collapsed into the empty hydrophobic cavity. Thus, the ns-LTP2 structure seems able to expand the hydrophobic cavity to accommodate the alkyl ligand. These liganded and unliganded ns-LTP2 structures have two cavities separated by the same septum formed by residues 7, 14 and 28 (Fig. 8*b*).

As previously described (Samuel *et al.*, 2002; Pons *et al.*, 2003), rice and wheat ns-LTP2 are structurally homologous to ns-LTP1, constituting a family of related proteins. As illustrated in Fig. 8(*c*), their α-helical topology is well conserved and the four cysteine bridges, although having different pairing patterns, superimpose well. Both proteins are capable of binding two lipids using a different geometry. ns-LTP1 is characterized by a long tunnel-like cavity able to accommodate two lipids in a head-to-tail orientation (Charvolin *et al.*, 1999), while wheat ns-LTP2 has two adjacent hydrophobic cavities.

4. Discussion and conclusions

Plant ns-LTPs constitute a family of ubiquitous proteins that play essential roles

in lipid trafficking during biosynthesis of cuticle layers and in mobilization of seed-storage lipids during germination, as well as in defence signalling and inhibition of fungal infections. Most of the data on the three-dimensional structures of ns-LTPs and their lipid-binding properties concern ns-LTP1. The lipid-transfer activity of ns-LTP2 was first observed for wheat and rice ns-LTP2 (Douliez *et al.*, 2001; Monnet *et al.*, 2001; Samuel *et al.*, 2002). Here, we report the high-resolution structure of the wheat ns-LTP2 protein and the elucidation of the three-dimensional arrangement of its two lipid-binding sites. These data provide a solid basis for understanding the promiscuous lipid-binding properties of this family of proteins.

4.1. Cavities and lipid-binding properties

The protein fold stabilized by four strictly conserved cysteine bridges and an extensive hydrogen-bonding network could be extended to all members of the ns-LTP2 subfamily. This highly stable structural motif with an α-helical bundle structure delineates a main central hydrophobic cavity and a secondary smaller cavity. The rigidity of this fold also ensures that these hydrophobic cavities are present in the free form of the rice and wheat ns-LTP2. However, there is evidence indicating that these proteins retain a fair amount of residual flexibility in their C-terminal segment. A significant change in the shape and volume of the main cavity is induced by a C-terminal backbone shift and limited reorganization of bordering amino-acid side chains. This typical plasticity of the ligand-binding cavity could provide the structural basis for explaining the non-specificity of these ns-LTP2 proteins. Invariant and conservatively exchanged hydrophobic residues line these two deep lipid-binding pockets, separated by a conserved septum defined by the side chains of residues Leu7, Ile14 and Leu28. This septum is also observed in the uncomplexed rice ns-LTP2 (Samuel *et al.*, 2002). Thus, it seems very unlikely that any reorientation of these residues could induce the formation of a continuous hydrophobic binding-pocket analogue to the tunnel of ns-LTP1s. The analysis of this crystal structure of wheat ns-LTP2 complexed with two LPG lipids also reveals that the hydrophobic fatty-acid chains are deeply buried in distinct cavities and generate a tightly packed hydrophobic core that further contributes to the stabilization of the protein. The polar head group of LPG in the secondary cavity is exposed to solvent and disordered as it lies along a basic solvent-exposed groove at the entrance of the main pocket.

4.2. Dimeric assembly

The packing of proteins in the crystal shows tight contacts through a twofold crystallographic axis, suggesting the presence of a dimeric quaternary structure in solution. Although initially proposed to be a monomer in solution (Pons *et al.*, 2003), the protein assembles as a dimer in the crystal. This could be explained by high protein concentration in the crystallization drops, the presence of lipid ligand and neutral pH. Thus, our data suggest that wheat ns-LTP2 could exist under physiological conditions in a monomer–dimer equilibrium. However, its functional relevance has not been addressed directly in this study and remains to be established. This oligomeric assembly is of interest as it could drive the multivalent interaction with diacylated lipid ligands.

4.3. Biological implications

The present results show that wheat ns-LTP2 has secondary and tertiary structures analogous to those of the ns-LTP1 family. Even though it is known to bind various lipids, the biological significance of these interactions is not fully understood. Based on hydrophobic matching properties, the major binding site of wheat ns-LTP2 seems to be optimized for a broad range of fatty-acid lengths from ten to 18 C atoms. A longer chain could not be accommodated into the hydrophobic channel and thus such extra C atoms protrude into the water outside the protein. The binding of such lipids will become increasingly unfavourable energetically. The shape of the binding cavity appeared also to accommodate the kink of monounsaturated fatty acids such as palmitoleic or oleic acids. The secondary binding site has room for shorter fatty acids (8–14 C atoms) threading through the hydrophobic cavity.

An interesting question concerns the mechanisms of capture/release of the lipid ligands. In the case of ns-LTP1, the lipid ligand could enter at either end of the hydrophobic channel, depending on the protein and/or the ligand, with opposite orientation in barley and maize nsLTP1s (Lerche *et al.*, 1998) or as two molecules lying in a head-to-tail orientation in wheat ns-LTP1 (Charvolin *et al.*, 1999). This is not the case for the wheat ns-LTP2, where the long tunnel is split into two separate hydrophobic cavities ending with a common wall. There is no evidence for a movable lid of the type that regulates access to the ligand-binding cavity of elicitins (Boissy *et al.*, 1999) and certain lipases (Derewenda & Sharp, 1993). The conserved residues Lys40 or Arg54 in extended conformation at the entrance of the main cavity could open or close the access to the cavity. These basic amino acids could attract the carboxyl group or phosphate head of the lipids. After this initial electrostatic interaction, the palmitoyl chain could diffuse into the hydrophobic cavity with only minor hindrance.

Our crystal structure provides a basis for the analysis of the functional consequences of the sequence variability in the ns-LTP2 family. It is also a good model for examining lipid–protein interactions and the structural plasticity of the cavities by protein engineering, *i.e.* by the design of mutants that disrupt the geometry of the lipid-binding pockets in order to accommodate larger lipids or to create a tunnel-like cavity similar to that of the ns-LTP1 proteins.

We acknowledge Philippe Carpentier and the staff at beamline BM14 of the European Synchrotron Radiation Source Facility (ESRF, Grenoble) for their assistance with data collection, Jean-Marc Strub for performing mass-spectrometry analysis and Marie-Pierre Duviau for the preparation of protein samples.

References

Bahadur, R. P., Chakrabarti, P., Rodier, F. & Janin, J. (2004). *J. Mol. Biol.* **336**, 943–955.

Blein, J. P., Coutos-Thevenot, P., Marion, D. & Ponchet, M. (2002). *Trends Plant Sci.* **7**, 293–296.

Blessing, R. H. & Smith, G. D. (1999). *J. Appl. Cryst.* **32**, 664–670.

Boissy, G., O'Donohue, M., Gaudemer, O., Perez, V., Pernollet, J. C. & Brunie, S. (1999). *Protein Sci.* **8**, 1191–1199.

Buhot, N., Douliez, J. P., Jacquemard, A., Marion, D., Tran, V., Maume, B. F., Milat, M. L., Ponchet, M., Mikes, V., Kader, J. C. & Blein, J. P. (2001). *FEBS Lett.* **509**, 27–30.

Charvolin, D., Douliez, J. P., Marion, D., Cohen-Addad, C. & Pebay-Peyroula, E. (1999). *Eur. J. Biochem.* **264**, 562–568.

Collaborative Computational Project, Number 4 (1994). *Acta Cryst.* D**50**, 760–763.

Dasgupta, B., Pal, L., Basu, G. & Chakrabarti, P. (2004). *Proteins*, **55**, 305–315.

Dauter, Z., Dauter, M. & Dodson, E. (2002). *Acta Cryst.* D**58**, 494–506.

Dauter, Z., Dauter, M. & Rajashankar, K. R. (2000). *Acta Cryst.* D**56**, 232–237.

De Lamotte, F., Boze, H., Blanchard, C., Klein, C., Moulin, G., Gautier, M. F. & Delsuc, M. A. (2001). *Protein Expr. Purif.* **22**, 318–324.

DeLano, W. L. (2002). *The PyMOL Molecular Graphics System.* San Carlos, CA, USA: DeLano Scientific.

Derewenda, Z. S. & Sharp, A. M. (1993). *Trends Biochem. Sci.* **18**, 20–25.

Douliez, J. P., Michon, T., Elmorjani, K. & Marion, D. (2000). *J. Cereal. Sci. A*, **32**, 1–20.

Douliez, J. P., Pato, C., Rabesona, H., Molle, D. & Marion, D. (2001). *Eur. J. Biochem.* **268**, 1400–1403.

Garcia-Olmedo, F., Molina, A., Segura, A. & Moreno, M. (1995). *Trends Microbiol.* **3**, 72–74.

Gincel, E., Simorre, J. P., Caille, A., Marion, D., Ptak, M. & Vovelle, F. (1994). *Eur. J. Biochem.* **226**, 413–422.

Gomar, J., Petit, M. C., Sodano, P., Sy, D., Marion, D., Kader, J. C., Vovelle, F. & Ptak, M. (1996). *Protein Sci.* **5**, 565–577.

Han, G. W., Lee, J. Y., Song, H. K., Chang, C., Min, K., Moon, J., Shin, D. H., Kopka, M. L., Sawaya, M. R., Yuan, H. S., Kim, T. D., Choe, J., Lim, D., Moon, H. J. & Suh, S.W. (2001). *J. Mol. Biol.* **308**, 263–278.

Heinemann, B., Andersen, K. V., Nielsen, P. R., Bech, L. M. & Poulsen, F. M. (1996). *Protein Sci.* **5**, 13–23.

Hollenbach, B., Schreiber, L., Hartung, W. & Dietz, K. J. (1997). *Planta*, **203**, 9–19.

Jones, T. A., Zou, J. Y., Cowan, S. W. & Kjeldgaard, G. J. (1991). *Acta Cryst.* A**47**, 110–119.

Kader, J. C. (1996). *Annu. Rev. Plant Physiol. Plant Mol. Biol.* **47**, 627–654.

Kissinger, C. R., Gehlhaar, D. K. & Fogel, D. B. (1999). *Acta Cryst.* D**55**, 484–491.

Kleywegt, G. J. & Jones, T. A. (1994). *Acta Cryst.* D**50**, 178–185.

Laskowski, R. A., MacArthur, M. W., Moss, S. D. & Thornton, J. M. (1993). *J. Appl. Cryst.* **26**, 283–291.

Lee, J. Y., Min, K., Cha, H., Shin, D. H., Hwang, K. Y. & Suh, S. W. (1998). *J. Mol. Biol.* **276**, 437–448.

Lerche, M. H., Kragelund, B. B., Bech, L. M. & Poulsen, F. M. (1997). *Structure*, **5**, 291–306.

Lerche, M. H., Poulsen, F. M. & Selitrennikoff, C. P. (1998). *Protein Sci.* **7**, 2490–2498.

Leslie, A. G. W. (1999). *Acta Cryst.* D**55**, 1696–1702.

Lucke, C., Huang, S., Rademacher, M. & Ruterjans, H. (2002). *Protein Sci.* **11**, 2382–2392.

Maldonado, A. M., Doerner, P., Dixon, R. A., Lamb, C. J. & Cameron, R. K. (2002). *Nature (London)*, **419**, 399–403.

Marion, D., Douliez, J. P., Gautier, M. F. & Elmorjani, K. (2003). *Plant Food Allergens*, edited by E. N. C. Mills & P. R. Shewry, pp. 57–69. Oxford: Blackwell.

Merritt, E. A. (1999). *Acta Cryst.* D**55**, 1109–1117.

Molina, A., Diaz, I., Vasil, I. K., Carbonero, P. & Garcia-Olmedo, F. (1996). *Mol. Gen. Genet.* **252**, 162–168.

Molina, A. & Garcia-Olmedo, F. (1997). *Plant J.* **12**, 669–675.

Molina, A., Segura, A. & Garcia-Olmedo, F. (1993). *FEBS Lett.* **316**, 119–122.

Monnet, F. P., Dieryck, W., Boutrot, F., Joudrier, P. & Gautier, M. F. (2001). *Plant Sci.* **161**, 747–755.

Murshudov, G. N., Vagin, A. A. & Dodson, E. J. (1997). *Acta Cryst.* D**53**, 240–255.

Navaza, J. (1994). *Acta Cryst.* A**50**, 157–163.

Nicholls, A., Bharadwaj, R. & Honig, B. (1993). *Biophys. J.* **64**, 166–170.

Pato, C., Le Borgne, M., Le Baut, G., Le Pape, P., Marion, D. & Douliez, J. P. (2001). *Biochem. Pharmacol.* **62**, 555–560.

Perrakis, A., Sixma, T. K., Wilson, K. S. & Lamzin, V. S. (1997). *Acta Cryst.* D**53**, 448–455.

Petersen, M. T., Jonson, P. H. & Petersen, S. B. (1999). *Protein Eng.* **12**, 535–548.

Pons, J. L., de Lamotte, F., Gautier, M. F. & Delsuc, M. A. (2003). *J. Biol. Chem.* **278**, 14249–14256.

Read, R. J. (1986). *Acta Cryst.* A**42**, 140–149.

Samuel, D., Liu, Y. J., Cheng, C. S. & Lyu, P. C. (2002). *J. Biol. Chem.* **277**, 35267–35273.

Shin, D. H., Lee, J. Y., Hwang, K. Y., Kim, K. K. & Suh, S. W. (1995). *Structure*, **3**, 189–199.

Stapley, B. J. & Creamer, T. P. (1999). *Protein Sci.* **8**, 587–595.

Vagin, A. & Teplyakov, A. (1997). *J. Appl. Cryst.* **30**, 1022–1025.

Vaguine, A. A., Richelle, J. & Wodak, S. J. (1999). *Acta Cryst.* D**55**, 191–205.

Wallace, A. C., Laskowski, R. A. & Thornton, J. M. (1995). *Protein Eng.* **8**, 127–134.

Weeks, C. M. & Miller, R. (1999*a*). *Acta Cryst.* D**55**, 492–500.

Weeks, C. M. & Miller, R. (1999*b*). *J. Appl. Cryst.* **32**, 120–124.